Design and Laboratory Validation of a Grid-Interfaced Totem-Pole PFC Converter With PR Controller and Isolated Phase Modulated Converter for Solar-Powered Next-Gen EV Charging System

Kanimozhi K, Prabhakaran KOOTHU KESAVAN, Nagendrappa HARISCHANDRAPPA, and Venkatesaperumal B.

***Abstract*—This paper proposes a stationery reference frame proportional-resonant (PR) controller for current control of grid-tied converters in an EV charger application. Since it is a viable alternative to rotational reference frame PI compensators in AC applications, the PR controller has been adopted for achieving zero steady state error without using any computationally intensive reference frame transformations. In this paper, a method to design the structure of PR controller and its coefficients according to the desired transient behaviour of AC signal amplitude in PFC converter current loop has been proposed. The importance of suggested PR controller design method is that the grid current magnitude is varying constantly based on the available PV power and battery charger levels which necessitates the controller to act in desired transient behaviour. So, by this way the impact of variation in system parameters have been completely overcome by operating the converter controllers appropriately in a solar powered EV charger system. To verify the effectiveness of the proposed controller design, extensive simulations and experimental studies are performed in a 1.5 kW EV charger system under various PV irradiances and charger power levels. The experimental results obtained from the laboratory prototype confirms the simulation findings.**

***Index Terms*—Current control, electric vehicle charger, photovoltaic systems, power factor correction, proportional-resonant (PR) controller.**

I. Introduction

TOWARDS the goal of attaining sustainable future, induction of electric mobility is proliferating at faster rate in the transportation sector due to its attributes such as greater well to wheel efficiency, flexibility in adopting diversified energy resources, reduced greenhouse gas emissions etc. [1]. Traditionally, EV batteries are powered from the grid either through on-board or off-board charging system. As this would not offer a truly sustainable mobility, more focus is made on utilizing renewable energy sources (RES) to meet the EV charging demand [2]. Amongst the available RES, solar photovoltaic (PV) system is found to be a viable option as it is modular, compact, does not have rotating parts and hence low maintenance [3]–[4]. The general configuration of solar powered EV charging systems with three ports viz. PV, grid and EV battery is illustrated in Fig. 1. Here, boost converter controls PV power, battery charging/discharging is controlled by phase-shifted full bridge (PSFB) converter and a totem-pole power factor correction (PFC) converter controls the grid power. These converters are interfaced across the DC bus with DC link capacitor [5]. The considered three-port solar powered EV charger configuration possesses many advantages viz. effective utilization of PV power by transferring it as DC quantity [6], elimination of additional inverter for grid-integration [7], energy storage systems are not required to store PV power as it is taken care by EV battery [8], possible execution of intelligent power management algorithm to reduce the net operating cost of the charger system [9]. However, to utilize all these benefits, the effective implementation of control algorithms is essential to overcome the diurnal nature of PV and battery power in solar integrated charger system. In addition to that, the control strategies of the converters should also facilitate the seamless transition of various operating conditions such as G2V, V2G etc. in the charger system [10].

In literature, various converter topologies and control techniques are presented for solar powered EV charger systems. In [11], a control strategy to improve grid power quality is developed and in [12], an adaptive control to overcome the dynamics with PV and battery power is implemented. A PV fed EV battery charger possessing various modes of operation is developed in [13] whereas in [14], a unified control for a charger circuit is presented. A residential electric vehicle charger which caters the house hold loads are presented in [15] with experimental validation and in [16], a PV, battery,

Manuscript received August 23, 2024; revised November 15, 2024; accepted December 17, 2025. Date of publication March 30, 2025; date of current version December 31, 2024. This work was supported by Vision Group of Science and Technology (VGST), Government of Karnataka under Centre of Innovative Science, Engineering and Education (CISEE) scheme, Karnataka, India under the grant KSTePS/VGST/2021-22/CISEE/GRD-1012/151/2022-23/35. *(Corresponding author: Prabhakaran Koothu Kesavan.)*

K. K, N. Harischandrappa, and V. B. are with Department of Electrical and Electronics Engineering, National Institute of Technology, Karnataka, Surathkal, Mangalore-575025, India (e-mail: kanimozhi.217ee003@nitk.edu.in; nagendrappa@nitk.edu.in; bvperumal@nitk.edu.in).

P. K. Kesavan is with Renewable Energy Laboratory, Prince Sultan University, Riyadh 11586, Saudi Arabia (e-mail: k7prabhakaran@gmail.com).

Digital Object Identifier 10.24295/CPSSTPEA.2024.00029

TABLE I
STATE OF ART ON VARIOUS CONTROL STRATEGIES FOR GRID-TIED CONVERTERS IN SOLAR POWERED EV CHARGER SYSTEM

References	Connected sources/Loads	Control strategies	Current control in grid-connected converters	Current control feature	Current control based on desired transient response
[14]	Grid, PV, EV battery, Storage Battery	DC link voltage, MPPT, EV battery and storage battery charging/discharging	No	-	No
[18]	Grid, EV battery, Storage battery, Domestic loads	DC link voltage, PFC, EV battery and storage battery charging/discharging	Yes	Power factor correction	No
[15]	Grid, PV, EV battery	DC link voltage, MPPT, EV battery charging/discharging	No	-	No
[11]	Grid, PV, EV battery	DC link voltage, MPPT, EV battery charging/discharging	No	-	No
[4]	Grid, PV, EV battery	DC link voltage, PFC, EV battery charging/discharging	Yes	Power factor correction	No
[10]	Grid, PV, EV battery, Residential loads	DC link voltage, MPPT, EV battery charging/discharging, DG – Voltage, freque ncy, reactive power, mode switching	Yes	Power quality improvement	No
[13]	Grid, PV, EV battery, Storage battery	DC link voltage, EV battery charging/discharging, Storage battery charging/discharging, Reactive power	Yes	Power quality improvement	No
[19]	Grid, PV, EV battery	DC link voltage, PFC, Mode switching	Yes	Power factor correction	No
Proposed PR control	Grid, PV, EV battery	DC link voltage, PFC, MPPT, EV battery charging/discharging	Yes	Power factor correction	Yes

diesel generator-based EV charging station is developed. In [17], multiple mode of operation of the same charger system configuration is discussed with its control strategies whereas a multiport charger for light EVs with the ability to power the domestic appliances is developed in [18]. References [11]–[18], details the various control concepts and possible power flow capability of a solar powered EV charger system. Since PV power and battery charging/discharging levels may change constantly during a day, the development of control algorithms for the converters are playing crucial role in maintaining the stability of solar powered EV charger system. Further, this system necessitates that the grid-tied converter controller has to act according to the power requirement which has been decided from the available PV power and battery power [19]. So, designing the grid-tied converter controller is important in solar powered charger system, such that it should control based on the desired operating condition of the system. Table I provides the comprehensive review of the available literature in the area of solar power EV charger systems and its control strategies.

The aforementioned merits in designing the controllers of various power electronic converters have motivated the researchers around the globe to focus on this area. When power is exchanged with mains, grid side current control plays a vital role ensuring proper power exchange and also resolving the power quality issues [20]. In order to achieve zero steady-state current tracking error in case of ac excitation, proportional-integral (PI) control in synchronous frame is one of the preferred techniques [21]. But it suffers from sustainability issues when there is a demand for stationery-to-synchronous frame transformations [22]. Most of the above-mentioned drawbacks were remedied by introducing stationery frame proportional-resonant (PR) compensators which imposes near zero steady state error [23]. These PR controllers have been widely adopted in various field of applications viz. motor drives [24], dynamic voltage restorers [25], uninterruptable power system inverters [26], general grid-connected converters [27] and photo-voltaic converters [28]. A control strategy to achieve zero steady state error and the effect of the harmonics in ac current waveform is investigated in [29], for single phase PWM rectifiers whereas in [30], a control algorithm for three-phase grid-connected converter operating under grid voltage harmonics and asymmetry has been presented in [30].

In addition to that, the tuning of PR controller parameters using Lyapunov functions for single phase grid connected central inverters is presented in [31]. It guarantees the global stability of the converter system. A parameter tuning methodology for PR controllers using the design philosophy of the Ziegler-Nichols forced oscillation method is detailed in [32]. It includes tuning formula to provide accurate stability margin for each class of plant transfer function. In [33], the PR controller parameters are designed based on the selective pole-placement and cancellation method in voltage source inverters. It provides robust steady-state performance under different situations in the system. The importance of PR controller design for various applications are detailed in the literature. However, the design and development of PR controller for grid-tied converter in solar powered EV charging systems are not covered in the literature where the diurnal nature of PV power and battery power is crucial. This paper made an attempt to fill this gap by proposing a PR controller design based on the desired transient performance of the grid-tied converter in an EV charger system. Based on the above discussed context of the literature, the key contributions of this article are furnished below:

- Totem-pole PFC converter with PR controller to act based

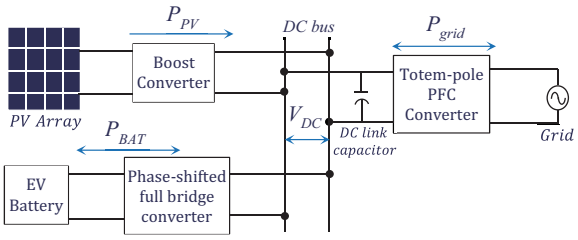

Fig. 1. Typical configuration of solar powered EV charger system.

on the desired transient behaviour has been proposed where the controller parameters have been designed with actual current control loop derived from the basic converter equations in solar powered EV charger systems.

- The effectiveness of proposed PR controller is that, there is a presence of additional resonant term in controller transfer function which effectively tracks the change in AC signal magnitude in current control possessing zero amplitude, frequency and phase steady-state error irrespective of the uncertainties in the charger system.
- The change in PV irradiances and battery power levels, changes the amplitude of grid current, which in turn accustom proposed PR controller parameters based on the desired transient behaviour.
- Totem-pole PFC converter with PR controller facilitates the power flow to happen from vehicle to grid operating conditions which becomes one of the essential operating modes in solar powered EV charger system.

The subsequent sections of the article are organized as follows: Section II deals with the system configuration and proposed control strategies for solar powered EV charger system. Section III details the current loop description of totem-pole PFC converter in a solar powered charger system. Section IV presents the design and development of PR controller based on desired transient behavior. The simulation and experimental results validating the stability analysis is provided in Section V. Finally, the conclusion is given is Section VI.

II. System Configuration of Solar Powered EV Charger Systems

For the typical solar powered EV charger systems shown in Fig. 1, the detailed power electronic circuitry is presented in Fig. 2(a) and the associated control strategy for the converters are shown in Fig. 2(b)-(d). Totem-pole PFC converter topology is one of the widely adopted configuration of PFC converter for an EV charging system as it has reduced switch count, low losses and bidirectional power transfer capability in comparison with the conventional active boost PFC topology. The control structure consists of two control loops, inner current control loop to regulate pure sinusoidal grid current and outer voltage control loop to regulate the DC link voltage. The reference voltage for voltage control is 400 V whereas the reference current for current control is generated from the grid voltage with the required amplitude form the real-time measured values of PV power and battery power. With these

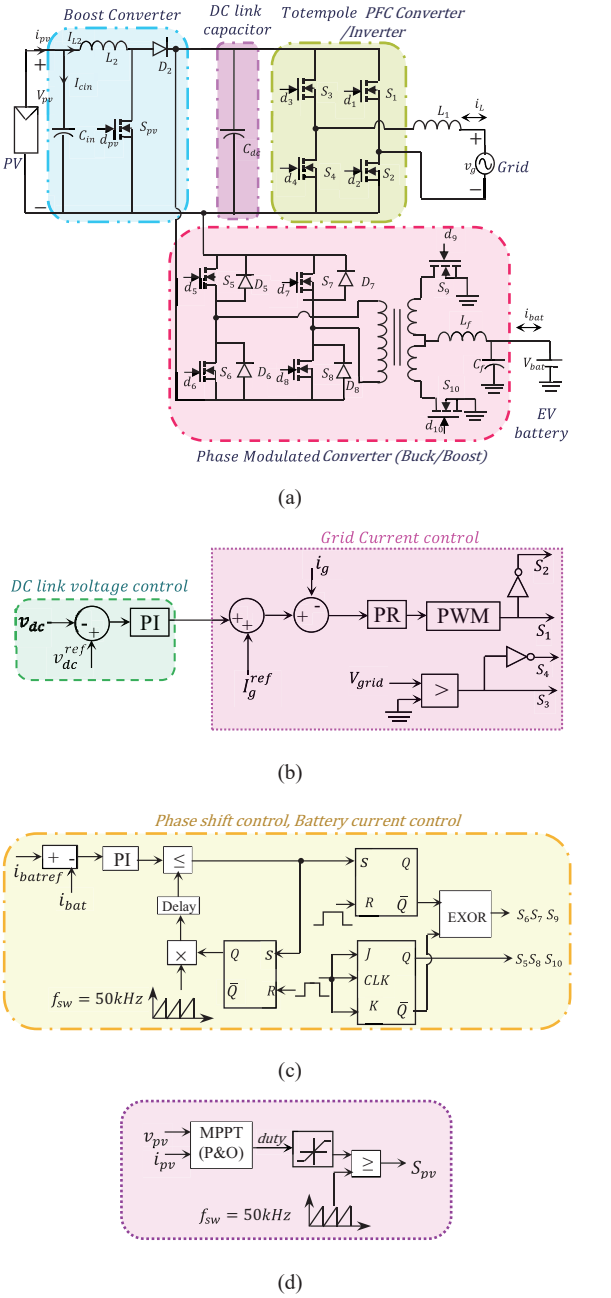

Fig. 2. (a) Detailed power electronic circuitry of solar powered EV charger system, Control strategy of (b) Totem-pole PFC converter, (c) Phase shifted full bridge converter, (d) PV boost converter.

reference values, outer voltage control loop regulates the actual value with PI controller and the inner current control loop regulates the actual value with PR controller, which will give appropriate gate pulses to the MOSFET switches S_1 and S_2. The switch S_4 and S_3 are operated at supply frequency during positive and negative half cycles respectively. Here, the grid current control needs to be implemented to maintain the power factor near unity irrespective of uncertainties like PV irradiance and battery charging levels in the charger system.

Phase-shifted full bridge converter control strategy is shown in Fig. 2(c). It is designed to achieve peak current control and battery charging control by operating the switches connected

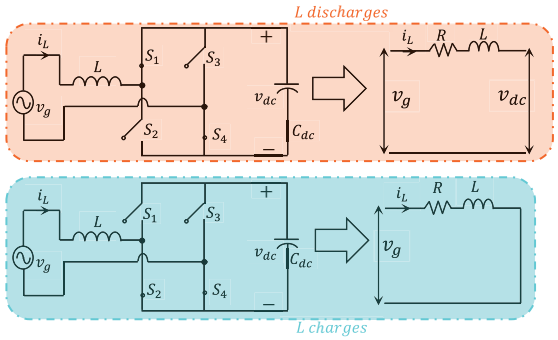

Fig. 3. Totem-pole PFC converter (a) Equivalent circuit representation, (b) Simplified representation for current loop.

with the primary and secondary side of the high frequency transformer. This reference current signal controls the actual battery current to behave accordingly using a PI controller and the phase shift is incorporated with the generated gate pulses by using SR and JK flipflop. With this phase shifted signals MOSFET switches S_5, S_6, S_7 and S_8 are getting operated. For PV fed boost converter, the MPPT operation of PV system is realized through the perturb and observe (P&O) method which modulates the duty cycle of the MOSFET switch S_{pv} of boost converter is shown in Fig. 2(d). The importance of operating PV at MPP is to utilize optimum PV power in an EV charger system, which is also used in generating the reference grid current for PFC converter. Since this work focuses on the grid-tied converter and its control strategy, the design and development of the proposed PR controller for PFC converter is detailed here.

With the above considerations, the objective of the proposed work is to design the PR controller parameters such that actual grid current has to follow the reference current signals even though there is a change in the amplitude of grid current. The following steps has been followed to derive the PR controller parameters of PFC converter based on the desired operating behaviour in the charger system. As an initial step, the current control loop of PFC converter with the influence of converter system parameters based on the switching position of MOSFET switches are derived. These derived equations detail the information about the requirement of feed-forward signals. The importance of these signals in solar powered charger system is that, it gives the present operating condition of PV and battery converter. Further as the next stage, the PR controller parameters are derived with the objective to have zero steady-state amplitude error and zero instantaneous phase error even though there is an occurrence of change in reference grid current generation. By adopting these steps, the PR controller parameters of PFC converter has been derived in the subsequent section.

III. Current Loop Description of Totem-Pole PFC Converter

The power electronics circuitry of totem-pole PFC converter shown in Fig. 2(a) is utilized to get the equivalent circuit

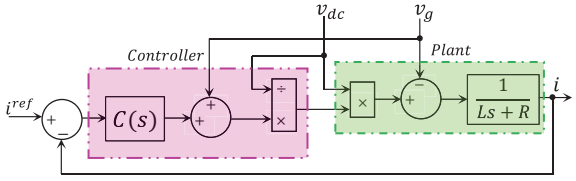

Fig. 4. Closed-loop system block diagram of Totem-pole PFC converter.

representation of the converter. Based on the ON and OFF state of the MOSFET switches S_1 and S_4 of PFC converter, the equivalent circuit representation is shown in Fig. 3(a). The averaged equivalent circuit of a generalized current loop of PFC converter are represented in Fig. 3(b). Here, v_{dc} represents the voltage across the DC link capacitor which is a controlled voltage whereas v_g is the grid voltage. The inductor L with its internal resistance R is represented as a separating impedance respectively. With the simplified current loop representation of PFC converter, the current loop dynamic equations are derived and it is given as (1) and (2).

$$L\frac{\mathrm{d}i_L(t)}{\mathrm{d}t} = v_{dc}(t) - Ri_L(t) - v_g(t) \tag{1}$$

$$L\frac{\mathrm{d}i_L(t)}{\mathrm{d}t} = -Ri_L(t) - v_g(t) \tag{2}$$

The closed loop block diagram of current control loop is shown in Fig. 4 which is presented from the derived current loop dynamic equation given as equations in (1) and (2). $C(s)$ represents the compensator transfer function which process the error signal between the reference current (i^{ref}) and the actual current (i). Here the DC link voltage (v_{dc}) and grid voltage (v_g) are assumed to be measurable and these signals have been used as a feed-forward signals to the controller and so the system dynamics can be decoupled from the external disturbances. Amplitude of i^{ref} has been computed based on the charger power levels and the available PV power. By having a feed-forward signals from PV converter and EV converter the dynamics in these values can be computed and variation in i^{ref} has been derived. Further, this has been fed into a compensator transfer function to get the desired transient response.

IV. PR Controller Design Based on Desired Transient Behaviour

The objective of designing the PR controller of Totem-pole PFC converter is that it should give zero-steady state amplitude error and zero instantaneous phase error so that desired transient behaviour irrespective of uncertainties in PV and EV system in a solar powered EV charger system can be achieved. Initially assume a linear time-invariant system which will generate the grid current reference signals as

$$i^{ref}(t) = A\sin(\omega_0 t)\, u(t) \tag{3}$$

The Laplace transformed representation of (3) is

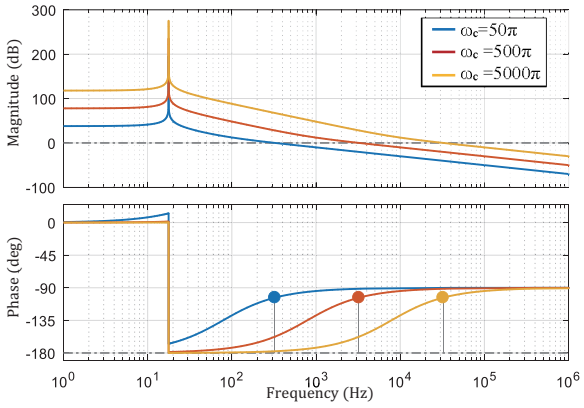

Fig. 5. Bode plot for loop gain of overall transfer function.

$$I^{\text{ref}}(s) = \frac{A\omega_0}{s^2 + \omega_0^2} \tag{4}$$

The desired time domain response of actual grid current has to be requested such that it possess zero steady state amplitude error with transient time constant of ω_c^{-1} and zero instantaneous steady state phase error. So, with this aim the desired grid current response has been defined as

$$i(t) = A(1 - e^{-\omega_c t})\sin(\omega_0 t)\, u(t) \tag{5}$$

In Laplace domain, the actual grid current has been derived as

$$\begin{aligned} I(s) &= \frac{A\omega_0}{s^2 + \omega_0^2} - \frac{A\omega_0}{(s+\omega_c)^2 + \omega_0^2} \\ &= \frac{A\omega_0}{s^2 + \omega_0^2} \cdot \frac{2\omega_c s + \omega_c^2}{(s+\omega_c)^2 + \omega_0^2} = I^{\text{ref}}(s) \cdot T(s) \end{aligned} \tag{6}$$

where $T(s) = \dfrac{I(s)}{I^{\text{ref}}(s)} = \dfrac{2\omega_c s + \omega_c^2}{(s+\omega_c)^2 + \omega_0^2}$.

Here, $T(s)$ represents the closed loop tracking transfer function which represents the overall transfer function of the plant and the controller is given as

$$T(s) = \frac{C(s)P(s)}{1 + C(s)P(s)} \tag{7}$$

where $C(s)$ represents the controller transfer function and $P(s)$ represents the plant transfer function respectively. By equating (6) and (7), the loop gain of the transfer function has been computed is shown below as

$$L(s) = C(s)P(s) = \frac{2\omega_c s + \omega_c^2}{s^2 + \omega_0^2} \tag{8}$$

Loop gain of the transfer function relates the parameters ω_c and ω_0. The value of ω_0 has been known as 100 π and for various values of ω_c the bode plot has been plotted in Fig. 5 to understand the relation between the parameters. From Fig. 5, it has been observed that when ω_c increases, then the phase margin has been reduced. From (8), the PR controller

TABLE II
CIRCUIT PARAMETERS

Parameter	Value
Grid voltage	230 V
Line frequency	50 Hz
Switching frequency	50 kHz
Diode forward voltage V_{dpv}	0.8 V
Totem-pole PFC inductor L_1	1.32 mH
PV boost inductor L_2	0.88 mH
DC link Capacitor C_o	1200 µF
PV input Capacitor C_{in}	400 µF
Filter Inductor L_f	105 µH
Filter Capacitor C_f	15 µF
DC link voltage	400 V
Charger power rating	1.5 kW

transfer function in terms of the system parameters has been derived as

$$C(s) = P(s)^{-1} \cdot \frac{2\omega_c s + \omega_c^2}{s^2 + \omega_0^2} \tag{9}$$

By substituting the plant transfer function of totem-pole PFC converter the controller transfer function is derived as

$$C(s) = (Ls + R) \cdot \frac{2\omega_c s + \omega_c^2}{s^2 + \omega_0^2} \tag{10}$$

The proportional and resonant terms of the PR controller can be easily identified using (10), and it is computed that the parameter values are depended on the system parameters.

The designed PR controller parameters are

$$C(s) = K_P + \frac{K_{R1} s}{s^2 + \omega_0^2} + \frac{K_{R2}}{s^2 + \omega_0^2} \tag{11}$$

$$\begin{cases} K_P = 2L\omega_c \\ K_{R1} = L\omega_c^2 + 2R\omega_c \\ K_{R2} = R\omega_c^2 - 2L\omega_c\omega_0^2 \end{cases} \tag{12}$$

From (12), it is clear that the derived PR controller possess an additional term K_{R2} with the conventional PR controller parameters K_P and K_{R1}. Also, to derive the proposed PR controller parameters the converter parameters need to be known as an initial stage. The PFC converter ratings of a solar powered EV charger system is detailed in Table II. With these details the PFC converter inductor and its DCR value is designed such that it should provide stable power for various values of irradiances in the charger system. To provide continuous conduction mode operation over one switching period, input inductor value of PFC converter is obtained as

$$L = \frac{1}{\Delta I_{Lg}} \cdot \frac{v_s^2}{P_o}\left(1 - \frac{\sqrt{2}\cdot v_s}{v_{dc}}\right) \cdot T_S = 0.53 \text{ mH} \tag{13}$$

The DCR value of the inductor is calculated as 0.052 Ω. From these L and C values, the PR controller parameters are designed and the corresponding values are given in Table

TABLE III
PR CONTROLLER PARAMETERS

Controller Parameter	Value
K_P	0.16
K_{R1}	29
K_{R2}	−15150

TABLE IV
SWITCH CONDITIONS FOR VARIOUS OPERATING STATES OF TOTEM-POLE PFC CONVERTER

Operating states	Switch Condition			
	S_1	S_2	S_3	S_4
State 1	OFF	ON	OFF	ON
State 2	ON	OFF	ON	OFF

TABLE V
PV ARRAY SPECIFICATIONS AT STC

Parameter	Value
Short circuit current (I_{sc})	8.68 A
Open circuit voltage (V_{oc})	37.6 V
Current at MPP (I_{mp})	8.1 A
Voltage at MPP (V_{mp})	30.9 V
Maximum power	250.29 W
Number of modules in series	5

III. With the designed parameters the controller transfer function $G_c(s)$ can be easily derived and further to examine the effectiveness of the proposed design the transient analysis has to be performed from the small signal model of totem-pole PFC converter. For deriving the mathematical model of totem-pole PFC converter, the differential equations are linearized around steady state operating point and the small signal model has been derived as an initial step. Based on the position of the MOSFET switches the number of operating states of the totem-pole PFC converter has been identified and it is given in the Table IV. Here, during positive half cycle, S_4 is ON and based on values of S_1 the switch conditions of S_1, S_2 will change continuously. During negative half cycle, S_3 is ON and the rest of switches S_1, S_2 operates in similar fashion. Initially during positive half cycle, the operation of MOSFET switches for one switching cycle has been taken into consideration for deriving the mathematical equations in totem-pole PFC converter. In this work, the inductor current equations have been derived during these two operating states and it is detailed below.

State 1:

$$\frac{\mathrm{d}i_{L1}}{\mathrm{d}t} = i_{L1}\left(\frac{-R_{L1}}{L_1}\right) + \frac{v_g}{L_1} \tag{14}$$

State 2:

$$\frac{\mathrm{d}i_{L1}}{\mathrm{d}t} = i_{L1}\left(\frac{-R_{L1}}{L_1}\right) + \frac{v_g}{L_1} - \frac{v_{dc}}{L_1} \tag{15}$$

The derived equations are time weighed and averaged over one switching cycle to obtain the small signal model and from the model the transfer function is derived and it is given below.

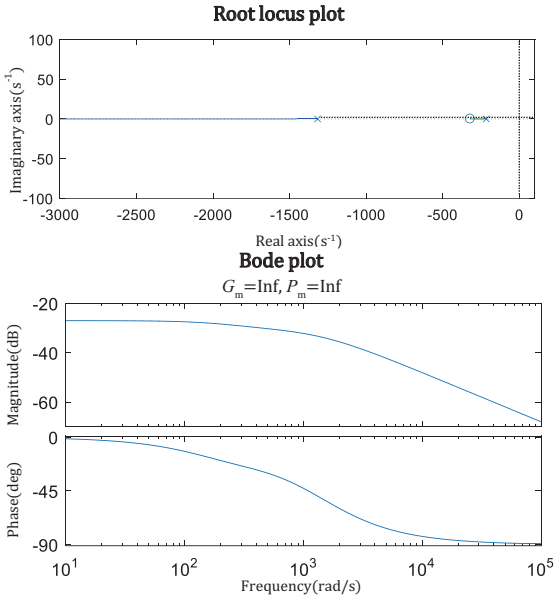

Fig. 6. Root-locus plot and bode plot of $\frac{\widehat{l_{L1}}(s)}{\widehat{d}_1(s)}$.

$$\frac{\widehat{l_{L1}}(s)}{\widehat{d}_1(s)} = \frac{512\times10^3\times(s+321.7)}{12.9\times10^3\times s^2+1.98\times10^7\times s+3.685\times10^9} \tag{16}$$

For the derived transfer function, the root locus plot and the bode plot has been plotted to analyse the stability of the system is shown in Fig. 6. It can be observed from Fig. 6 that the system is open loop stable and the following points are inferred about the stability of the system.

1. Eigen values of all the system transfer functions are negative and further zeroes are also placed on the left half of the s-plane. This states that the system is absolutely stable.
2. The phase margin (P_m) and gain margin (G_m) values from the bode plots of the transfer function in Fig. 6 also validates the stability of the system.

The stability analyses are performed and it is proved that the system is open loop stable, so that the system provide stable operation for closed loop system also.

To analyze the system stability, the overall transfer function $G(s)$ is computed as $G_c(s)\cdot\frac{\widehat{l_{L1}}(s)}{\widehat{d}_1(s)}$. For the derived transfer function, the step response is observed to get the information about time domain specifications such as delay time, rise time, peak time and peak overshoot. Since the objective of the proposed controller is to effectively track the reference value within a short span of time, the influence of these parameters plays a key role in this system configuration. The observed step response of the overall transfer function is detailed in Fig. 7. To examine the time domain parameters, the unit step signal

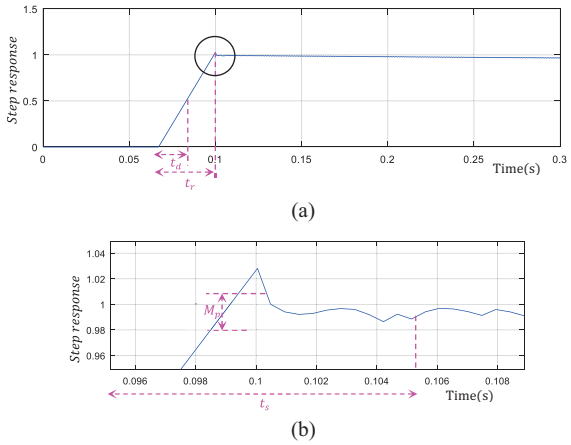

Fig. 7. (a) Step response of overall transfer function $G_c(s)\cdot\dfrac{\widehat{I_{L1}}(s)}{\widehat{d_1}(s)}$, (b) Zoomed in of (a).

is initiated at t = 0.07 s and the delay time is observed to be 0.01 s and rise time is observed to be 0.03 s in Fig. 7(a). To perceive the settling time and peak overshoot the zoomed in portion of the step response is shown in Fig. 7(b). It is found that the settling time is 0.035 s and the peak value is limited to 0.03% of the given input signal. It has been proven from these observations that effective tracking is achieved within a short span of time in the proposed PR controller. By this way, the controller should be capable to track the reference current even though it is subjected to variation in the amplitude of reference current generation in totem-pole PFC converter. Since, there is more possibility for continuous variation in amplitude of reference current generation in PFC converter controller there is a necessity that the controller should act accordingly. With these objectives, this methodology is proposed for designing the PR controller parameters with desired transient behaviour in EV charging applications. Since this work is concerned towards the PR controller design, the PI controller parameters of voltage control loop of totem-pole PFC converter and phase-shifted full bridge converter is derived using small signal analysis and it is detailed in Table VI for a grid-interfaced solar-powered EV charger system.

V. Results and Discussions

To validate the effective tracking of reference signals in PFC converter with proposed PR controller design methodology, a 1.5 kW solar powered EV charger system has been taken into consideration. Also, to verify the robustness of derived PR controller parameters the change in amplitude of reference grid current signal is occurred due to change in the PV irradiances and the battery power levels of an EV charger system. A dedicated MATLAB/Simulink model is developed to carry out the simulation of the circuit topology and control algorithm in Fig. 2 with designed PR controller parameters derived in preceding section. The experimentation is carried out in a 1.5 kW laboratory prototype that is built to examine the stability of the charger. The circuit parameters are given in Table II and the specifications of PV system are listed in Table V. The effective

TABLE VI
PI Controller Parameters

Totem-pole PFC Converter		Phase Shifted Full Bridge Converter	
G2V (Voltage control)	V2G (Voltage control)	G2V (Current control)	V2G (Current control)
K_p = 5999	K_p =520	K_p = 1562.8	K_p =3288
K_i = 599.9	K_i =52	K_i = 156.2	K_i =328.8

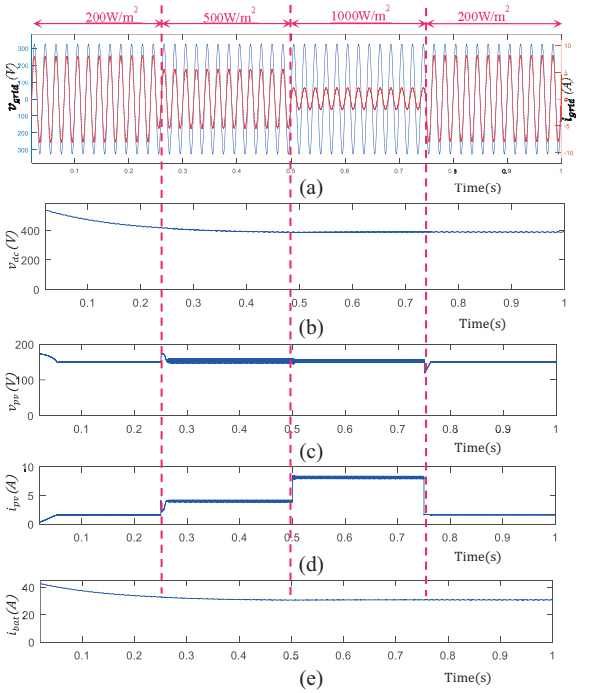

Fig. 8. Performance of solar powered EV charger system during change in PV irradiances.(a) Grid current, (b) DC link voltage, (c) PV voltage, (d) PV current, (e) Battery current.

implementation of grid current PFC control is tested for various cases involving dynamics in PV irradiance and battery power level.

A. Change in PV Irradiances for Constant Battery Power

The simulation model for 1.5 kW EV charger is developed with the proposed PR control algorithm for totem-pole PFC converter in a solar powered EV charger system. The system performance under various insolation conditions is observed and the key waveforms are shown in Fig. 8. It can be seen that initially at t = 0 s, the system is turned on with 200 W/m^2 irradiance then it is changed to 500 W/m^2 at t = 0.25 s which made the change in the reference magnitude of grid current. In Fig. 8(a), grid current possesses UPF operation whereas in Fig. 8(b) DC link voltage is maintained to 400 V. The similar testing is done with the irradiance of 1000 W/m^2 at t = 0.5 s and 200 W/m^2 at t = 0.75 s. The PV voltage and current waveforms for corresponding irradiance values are shown in Fig. 8(c) and (d). It is clear that the grid current amplitude is changing continuously at every instant of irradiance change. So, even though there is a change in a reference amplitude of grid

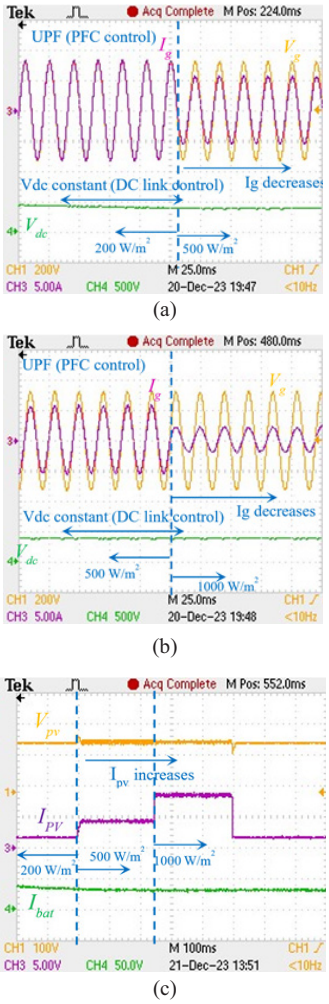

Fig. 9. Performance of solar powered EV charger system during change in PV irradiances. (a) Grid voltage, grid current and DC link voltage, (b) Grid voltage, grid current and DC link voltage, (c) PV voltage, PV current and battery current.

current, the actual grid current tracks the reference with zero amplitude, phase and frequency steady state error. This shows the effective operation of PR controller with the designed controller parameters. The considered change in PV irradiances is replicated as the PV current in Fig. 8(d). It is observed that for an increase in irradiance values, the grid current magnitude is reduced to maintain the battery power. This is because the controller has been set to meet the battery demand primarily from PV and the remaining deficient power by grid to obtain the power balance. The responses of battery and current levels are depicted in Fig. 8(e). The battery current response shows that continuous constant power is supplied to the battery load. This simulation results verify that the proposed controller is working as expected for a change in amplitude variation of grid current due to change in the PV irradiance *s* in solar powered charger systems.

The procedure is now repeated in experiment and results are shown in Fig. 9. It can be observed that for grid to vehicle power flow, the grid current waveform exhibits UPF with various irradiances such as 200 W/m^2, 500 W/m^2 and 1000 W/m^2 is shown in Fig. 9(a) and (b). It can also be noted that

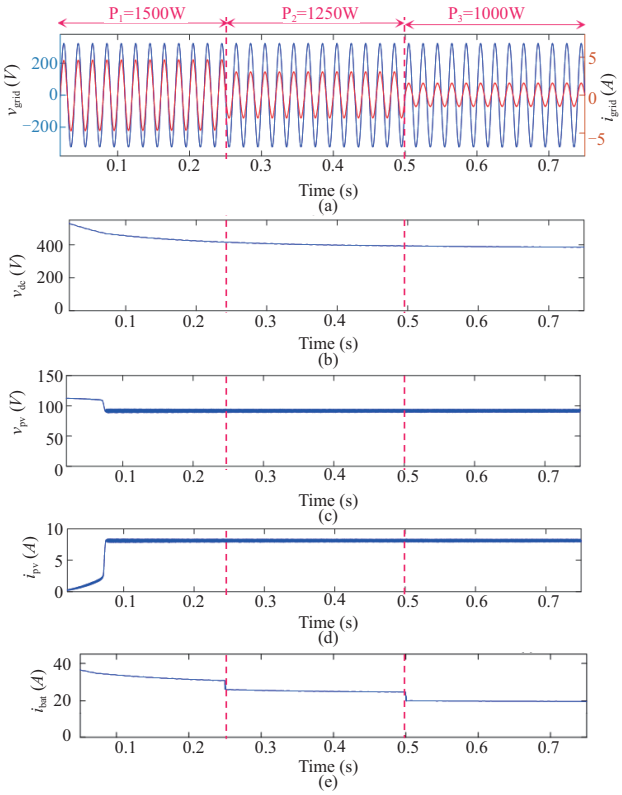

Fig. 10. Performance of solar powered EV charger system for various load conditions with G = 1000 W/m2. (a) Grid current, (b) DC link voltage, (c) PV voltage, (d) PV current, (e) Battery current.

when the insolation level varies, the PV converter controller effectively tracks the PV current and voltage corresponding to MPP. Accordingly, the PFC controller adjusts the grid current magnitude and hence the power drawn from the grid to achieve power balance. Further, it can also be noted that the DC link voltage in Fig. 9(a) and (b) and battery current in Fig. 9(c) is maintained to the reference values for various insolation levels. It is proven from these simulation and experimental waveforms that the controller is working effectively which tracks the expected parameters for various irradiance values.

B. Change in Battery Power With Constant Irradiance of G=1000 W/m^2

The responses of solar powered EV charger system for various battery power levels with G=1000 W/m^2 is detailed in Fig. 10. Since the rated battery power level is 1500 W, the three PV modules are connected in series, so the PV power operating at maximum power point is 750 W. The grid current response is shown in Fig. 10(a), where the grid current is synchronized with grid voltage and in Fig. 10(b) the DC link voltage is maintained to 400 V. This shows the effective operation of proposed PR controller for PFC converter during various battery power levels. The PV voltage and current responses for G = 1000 W/m^2 is shown in Fig. 10(c) and (d). The PV power is maintained to1250 W for G = 1000 W/m^2. The battery current levels are detailed in Fig. 10(e) for various change in power levels. From these waveforms it is observed that for various battery power levels, the grid current amplitude is varying for fixed irradiance value. In this case the change

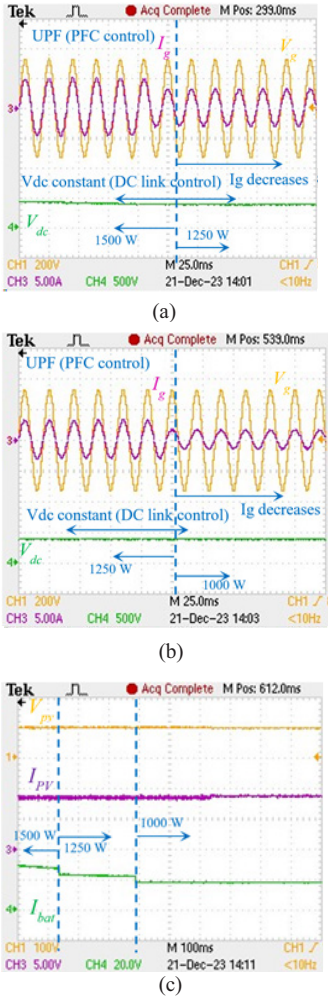

Fig. 11. Performance of solar powered EV charger system for various load conditions with G = 1000 W/ m^2. (a) Grid voltage, grid current and DC link voltage, (b) Grid voltage, grid current and DC link voltage, (c) PV voltage, PV current and battery current.

in amplitude of grid current takes place due to the change in battery power levels. So, the proposed PR controller has to make the actual grid current to effectively track the reference grid current even though there is a change in the grid current amplitude. This achieves the zero steady state error. From these responses it is clear that the controller is working effectively when there is a change in battery power levels.

The same procedure is repeated experimentally, and the measured waveforms are shown in Fig. 11. It is to be noted that, when there is a change in battery power levels, the grid current magnitude is varying to supply the load during constant PV irradiance of 1000 W/m^2. The shows the adaptiveness of proposed PR controller when there is a variation in change in battery power levels.

C. Change in PV Irradiances During Vehicle to Grid Operating Condition

The responses of solar powered charger system when the power flow happens in vehicle to grid operating condition is observed and the waveforms are shown in Fig. 12. In this

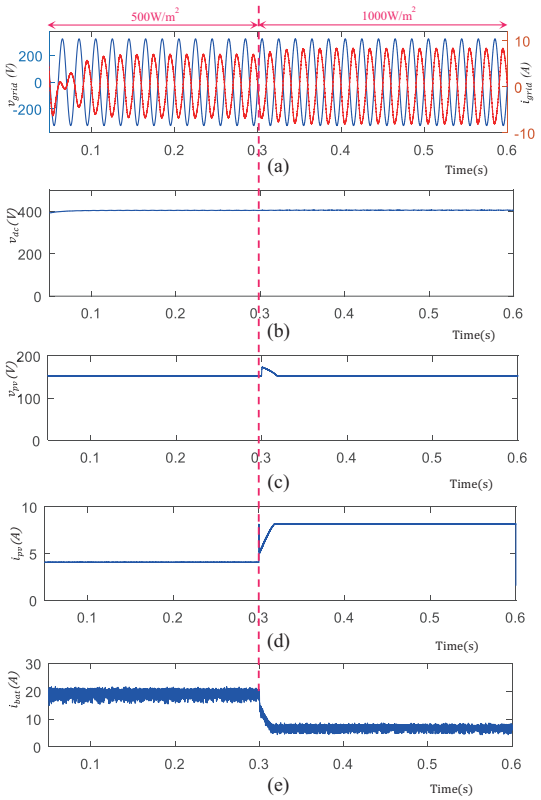

Fig. 12. Performance of solar powered EV charger system during vehicle to grid operating condition for various irradiances.(a) Grid current, (b) DC link voltage, (c) PV voltage, (d) PV current, (e) Battery current.

condition the PV and battery power is pumped into the grid. It can be seen that initially at t= 0 s, the system is turned on with 500 W/m^2 irradiance then it is changed to 1000 W/m^2 at t = 0.3 s. The grid current is out of phase with grid voltage in Fig. 12(a) indicates that the power from PV and battery is pumped into the grid. Also, the DC link voltage is maintained to 400 V. The PV voltage and current waveforms for corresponding irradiance values are shown in Fig. 12(c) and (d). It is clear that the grid current amplitude is changing when the irradiance changes. So, even though there is a change in a reference amplitude of grid current, the actual grid current tracks the reference with zero amplitude, phase and frequency steady state error. This shows the effective operation of PR controller with the designed controller parameters. The response of battery current is depicted in Fig. 12(e). The battery current response shows that battery discharging rate is reduced as irradiance increases. This simulation results verify that the proposed controller is working as expected for a change in amplitude variation of grid current due to change in the PV irradiances in solar powered charger systems. The experimental waveforms for this operating condition are shown in Fig. 13.

Grid current is out of phase with grid voltage, PV current increases as irradiance increases and DC link voltage is maintained to reference value. By this way, the experimental waveforms confirm that the simulation results and the converter controllers are working as expected during vehicle to grid operating condition. From these responses it is clear that the proposed PR controller is working effectively even

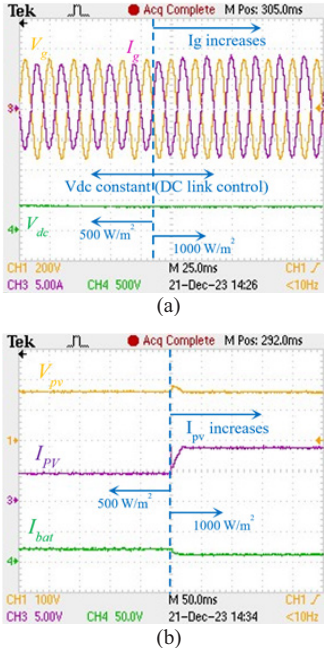

Fig. 13. Performance of solar powered EV charger system during vehicle to grid operating condition for various irradiances. (a) Grid voltage, grid current and DC link voltage, (b) PV voltage, PV current and battery current.

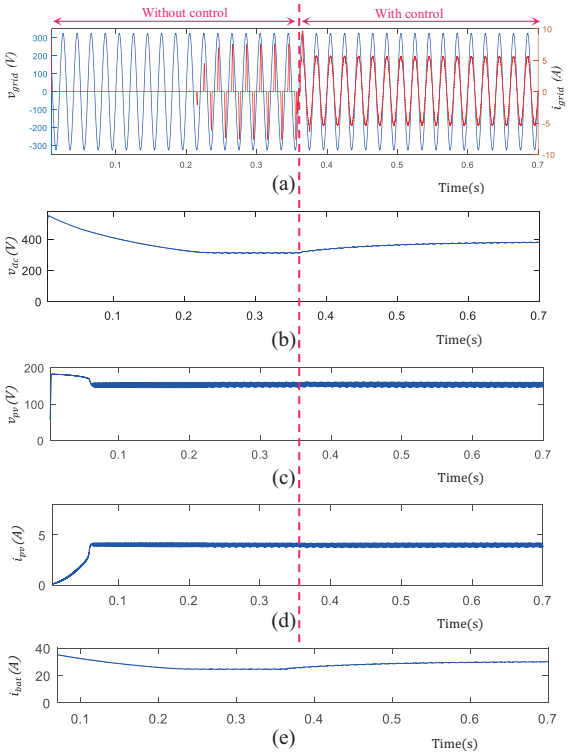

Fig. 14. Performance of an EV charger without control and with PR control case with constant irradiance of G = 500 W/m^2. (a) Grid current, (b) DC link voltage, (c) PV voltage, (d) PV current, (e) Battery current.

Fig. 15. Experimental setup with (a) PV-boost converter circuitry, (b) PSFB converter circuitry, (c) Totem-pole PFC converter circuitry, (d) L Filter (e) load, (f) Microcontroller- TMS320F28027F, (g) AC power supply, (h) DSO, (i) PV Simulator.

though there is a change in the amplitude of grid current due to change in PV irradiances and the battery power levels. Further to realize the effectiveness of the proposed PR control for grid-connected converters, the simulation has been performed for the case with and without control during constant irradiance of 500 W/m^2 and the performance of solar powered EV charger system is detailed in Fig. 14(a)-(e). It is observed that, the grid current waveform in Fig. 14(a), is working as expected which is in phase with grid voltage as soon as the control is initiated. This clearly shows the effective operation of proposed PR controller for grid-connected converters in solar powered EV charger system. The detailed comparison of the proposed controller with the existing control strategies in terms of various parameters and the conditions in solar powered EV charger system is detailed in Table VII. The developed laboratory setup to carry out the experimental results is shown in Fig. 15. Chroma PV simulator is used as a PV array with 5 PV modules connected in series. The output of the PV simulator is connected to a 1.25 kW boost converter. The grid-side totem-pole PFC converter and isolated DC-DC converter are designed for 1.5 kW power rating with the hardware circuit parameter details given in Tables II and V. By this way, the aim of deriving PR controller parameters based on transient behavior has been effectively utilized in solar powered EV charger system where the parameters are continuously varying. It is proven from the simulation results that the adopted PR controller for totem-pole PFC converter is effectively operate the charger system to adapt based on the real-time measured values in the system.

VI. Conclusion

In this article, the derivation of PR controller parameters based on the desired transient behavior of grid-tied converter in solar powered EV charger systems has been presented. Based on the AC signal amplitude of the PFC converter current loop the PR controller parameters is derived. In addition to

TABLE VII
COMPARISON OF PR CONTROLLER WITH EXISTING CONTROL STRATEGIES IN EV CHARGER APPLICATIONS

Parameters/Conditions	[13]	[14]	[15]	[4]	[18]	[10]	Proposed controller
Grid Current THD	<5%	-	<5%	<5%	-	<5%	<5%
PV uncertainty	Considered	Considered	Considered	Considered	Not Considered	Considered	Considered
Change in battery power	Yes	Yes	Considered	Considered	Considered	No	Considered
V2G	Yes	No	Yes	No	No	Yes	Yes
Closed loop stability analysis	No	No	No	No	No	No	Yes
Settling time	No	No	No	No	No	No	Yes (0.035 s)
Peak overshoot	No	No	No	No	No	No	Yes (0.03%)

that, the designed PR controller leads to give zero amplitude, frequency and phase steady-state error irrespective of the uncertainties in the charger system. The advantage of deriving the controller parameters in this aspect for a solar powered EV charger system is that, the battery power levels and the PV irradiances are constantly varying and so the controller has to act accordingly with the desired system behaviour. Further, the proposed PR controller design possess better transient behaviour in terms of time domain specifications such as settling time, rise time and peak overshoot. Simulation results in MATLAB/Simulink reveals that proposed charger configuration works satisfactorily in various operating conditions irrespective of PV dynamics and power levels. Finally, the experimental performance of a 1.5 kW EV battery charger system with the proposed control strategy has been examined for various operating conditions. The veracity of proposed PR control strategy of totem-pole PFC converter together with the PV and EV converter control algorithms has also been verified during various operating conditions which confirms the efficacy of the proposed controller configuration for solar powered charger systems.

References

[1] M. Ehsani, K. V. Singh, H. O. Bansal, and R. T. Mehrjardi, "State of the art and trends in electric and hybrid electric vehicles," in *Proceedings of the IEEE*, vol. 109, no. 6, pp. 967–984, Jun. 2021.

[2] P. M. deQuevedo, G. Muñoz-Delgado, and J. Contreras, "Impact of electric vehicles on the expansion planning of distribution systems considering renewable energy, storage, and charging stations," in *IEEE Transactions on Smart Grid*, vol. 10, no. 1, pp. 794–804, Jan. 2019.

[3] P. Denholm, M. Kuss, and R. M. Margolis, "Co-benefits of large-scale plugin hybrid electric vehicle and solar PV deployment," in *Journal of Power Sources*, vol. 236, pp. 350–356, Aug. 2013.

[4] N. Kumar, V. Saxena, B. Singh, and B. K. Panigrahi, "Power quality improved grid-interfaced PV assisted onboard EV charging infrastructure for smart households consumers," in *IEEE Transactions on Consumer Electronics*, vol. 69, no. 4, pp. 1091–1100, Nov. 2023.

[5] V. Monteiro, J. G. Pinto, and J. L. Afonso, "Experimental validation of a three-port integrated topology to interface electric vehicles and renewables with the electrical grid," in *IEEE Transactions on Industrial Informatics*, vol. 14, no. 6, pp. 2364–2374, Jun. 2018.

[6] G. R. Chandra Mouli, P. Bauer, and M. Zeman, "System design for a solar powered electric vehicle charging station for workplaces," in *Applied Energy*, vol. 168, pp. 434–443, Apr. 2016.

[7] G. R. C. Mouli, M. Leendertse, V. Prasanth, P. Bauer, S. Silvester, and S. van de Geer, "Economic and CO_2 emission benefits of a solar powered electric vehicle charging station for workplaces in the Netherlands," in 2016 *IEEE Transportation Electrification Conference and Expo (ITEC), Dearborn*, MI, USA, 2016, pp. 1–7.

[8] G. Carli and S. S. Williamson, "Technical considerations on power conversion for electric and plug-in hybrid electric vehicle battery charging in photovoltaic installations," in *IEEE Transactions on Power Electronics*, vol. 28, no. 12, pp. 5784–5792, Dec. 2013.

[9] G. R. C. Mouli, P. Bauer, and M. Zeman, "Comparison of system architecture and converter topology for a solar powered electric vehicle charging station," in *2015 9th International Conference on Power Electronics and ECCE Asia (ICPE-ECCE Asia), Seoul, Korea (South)*, 2015, pp. 1908–1915.

[10] S. Kumar, T. Upadhyay, and O. H. Gupta, "Power quality improvement and signal conditioning of PV array and grid interfaced off-board charger for electric vehicles with V2G and G2V capabilities," in *Chinese Journal of Electrical Engineering*, vol. 9, no. 4, pp. 132–143, Dec. 2023.

[11] V. Monteiro, J. G. Pinto, and J. L. Afonso, "Experimental validation of a three-port integrated topology to interface electric vehicles and renewables with the electrical grid," in *IEEE Transactions on Industrial Informatics*, vol. 14, no. 6, pp. 2364–2374, Jun. 2018.

[12] D. B. Wickramasinghe Abeywardana, P. Acuna, B. Hredzak, R. P. Aguilera, and V. G. Agelidis, "Single-phase boost inverter-based electric vehicle charger with integrated vehicle to grid reactive power compensation," in *IEEE Transactions on Power Electronics*, vol. 33, no. 4, pp. 3462–3471, Apr. 2018.

[13] R. K. Lenka, A. K. Panda, R. Patel, and J. M. Guerrero, "PV integrated multifunctional off-board EV charger with improved grid power quality," in *IEEE Transactions on Industry Applications*, vol. 58, no. 5, pp. 5520–5532, Sept.-Oct. 2022.

[14] V. Jain, B. Singh, and Seema, "A Grid connected PV array and battery energy storage interfaced EV charging station," in *IEEE Transactions on Transportation Electrification*, vol. 9, no. 3, pp. 3723–3730, Sept. 2023.

[15] A. Verma, B. Singh, A. Chandra, and K. Al-Haddad, "An implementation of solar PV array based multifunctional EV charger," in *IEEE Transactions on Industry Applications*, vol. 56, no. 4, pp. 4166–4178, Jul.-Aug. 2020.

[16] B. Singh, A. Verma, A. Chandra, and K. Al-Haddad, "Implementation of solar PV-battery and diesel generator based electric vehicle charging station," in *IEEE Transactions on Industry Applications*, vol. 56, no. 4, pp. 4007–4016, Jul.-Aug. 2020.

[17] A. Verma and B. Singh, "Multimode operation of solar PV array, grid, battery and diesel generator set based EV charging station," in *IEEE Transactions on Industry Applications*, vol. 56, no. 5, pp. 5330–5339, Sept.-Oct. 2020.

[18] S. Ghosh and B. Singh, "A multiport charger for light electric vehicles with function of powering domestic appliances," in *IEEE Transactions on Consumer Electronics*, vol. 70, no. 1, pp. 308–317, Feb. 2024.

[19] G. R. Chandra Mouli, P. Bauer, and M. Zeman, "System design for a solar powered electric vehicle charging station for workplaces," in *Applied Energy*, vol. 168, pp. 434–443, Apr. 2016.

[20] M. C. Mira, Z. Zhang, K. L. Jørgensen, and M. A. E. Andersen, "Fractional charging converter with high efficiency and low cost for electrochemical energy storage devices," in *IEEE Transactions on Industry Applications*, vol. 55, no. 6, pp. 7461–7470, Nov.-Dec. 2019.

[21] X. Zhao, C. Wang, R. Phukan, R, Burgos, S. Uicich, and P. Asfaux, "An enhanced modulation scheme for multi-level T-type inverter with loss balance and reduction," in *IEEE Transactions on Power Electronics*, vol. 38, no. 11, pp. 14050–14064, Nov. 2023.

[22] G. Tu, Y. Li, and J. Xiang, "Sliding mode control of energy storage sys-

tems for reshaping the accelerating power of synchronous generators," in *IEEE Transactions on Power Systems*, vol. 38, no. 2, pp. 1242–1256, Mar. 2023.

[23] X. Bao, F. Zhuo, Y. Tian, and P. Tan, "Simplified feedback linearization control of three phase photovoltaic inverter with an LCL filter," in *IEEE Transactions on Power Electronics*, vol. 28, no. 6, pp. 2739–2752, Jun. 2013.

[24] H. Nian, C. Wu, and P. Cheng, "Direct resonant control strategy for torque ripple mitigation of DFIG connected to DC link through diode rectifier on stator," in *IEEE Transactions on Power Electronics*, vol. 32, no. 9, pp. 6936–6945, Sep. 2017.

[25] A. Torres, P. Sanchez, and V. Battle, "A two degrees of freedom resonant control scheme for voltage sag compensation in dynamic voltage restorers," in *IEEE Transactions on Power Electronics*, vol. 33, no. 6, pp. 4852–4867, Jun. 2017.

[26] C. Wang, B. Liang, and J. He, "An enhanced power regulation and seamless operation mode transfer control through cooperative dual-interfacing converters," in *IEEE Transactions on Smart Grid*, vol. 9, no. 6, pp. 5576–5587, Nov. 2018.

[27] H. Komurcugil, N. Altin, S. Ozdemir, and I. Sefa, "Lyapunov-function and proportional-resonant-based control strategy for single-phase grid-connected VSI with LCL filter," in *IEEE Transactions on Industrial Electronics*, vol. 63, no. 5, pp. 2838–2849, May 2016.

[28] Y. Lu, W. Xiao, and D. D. -C. Lu, "Enhanced voltage regulation for PV power conversion using quasi-proportional resonant extended state observer," in *IEEE Journal of Emerging and Selected Topics in Industrial Electronics*, vol. 4, no. 1, pp. 70–77, Jan. 2023.

[29] C. Tang, K. Zhou, Y. Shu, Q. He, and Q. Chen, "Analysis and design of multiple resonant current control for grid-sonnected converters," in *IEEE Journal of Emerging and Selected Topics in Power Electronics*, vol. 10, no. 2, pp. 2539–2546, Apr. 2022.

[30] S. Wodyk and G. Iwanski, "Vibrating coordinates frame transformation based unity power factor control of a three-phase converter at grid voltage imbalance and harmonics," in *IEEE Transactions on Industrial Electronics*, vol. 69, no. 2, pp. 1114–1123, Feb. 2022.

[31] G. Jean-Pierre, N. Altin, A. E. Shafei, and A. Nasiri, "An expanded Lyapunov-function based control strategy for cascaded H-bridge multilevel active front-end converters," in *IEEE Open Journal of Power Electronics*, vol. 4, pp. 117–127, 2023.

[32] C. Lorenzini, L. F. A. Pereira, and A. S. Bazanella, "A generalized forced oscillation method for tuning proportional-resonant controllers," in *IEEE Transactions on Control Systems Technology*, vol. 28, no. 3, pp. 1108–1115, May 2020.

[33] B. Lin, L. Peng, and X. Liu, "Selective pole placement and cancellation for proportional–resonant control design used in voltage source inverter," in *IEEE Transactions on Power Electronics*, vol. 37, no. 8, pp. 8921–8934, Aug. 2022.

Kanimozhi K received the B.E. degree in electrical and electronics engineering from Anna University, Chennai, Tamil Nadu, India, and the M.S. degree in power systems from the National Institute of Technology, Tiruchirappalli, Tamil Nadu, India in 2012 and 2017, respectively. Currently, she is pursuing the Ph.D. degree in electrical and electronics engineering from the National Institute of Technology Karnataka, Surathkal, Mangalore, India. Her research interests include distributed generation, power electronics applications in electric vehicles and renewable energy systems.

Prabhakaran Koothu Kesavan received the B.Eng. degree in electrical and electronics engineering and the M. Eng. degree in power electronics and drives from Anna University, Chennai, India, in 2011 and 2013, respectively, and the Ph.D. degree in electrical and electronics engineering from the National Institute of Technology Karnataka, Surathkal, India, in 2019. He was a Postdoctoral Fellow with the Hydropower Simulation Laboratory, Department of Water Resource Development and Management, Indian Institute of Technology Roorkee, Roorkee, India. He subsequently worked as a Senior Lead Engineer in Electrical Systems at Aerostrovilos Energy Pvt. Ltd., a start-up associated with the Indian Institute of Technology Madras, India. From November 2022 to November 2024, he held the position of Postdoctoral Researcher in Renewable Energy at Prince Sultan University, Saudi Arabia. His research interests include nonlinear control, control of power converters, industrial drives, power electronics applications in renewable energy systems and power conditioning.

Nagendrappa Harischandrappa was born in the village Nakaralathanda, Bellary, India in 1977. He received the B.E. degree in electrical and electronics engineering and the M.Tech. degree in power and energy systems from the National Institute of Technology Karnataka (NITK), Surathkal, Mangalore, India, in 1999 and 2002, respectively, and the Ph.D. degree in electrical engineering from the University of Victoria, Victoria, BC, Canada, in 2015. He worked as an Assistant Lecturer from 2002 to 2004, and as a Teaching Fellow from 2004 to 2006, both with the Department of Electrical Engineering, NITK, Surathkal, where he is currently working as an Associate Professor. For a short period, he was an Assistant Engineer (operation and maintenance) with the Power Distribution Utility, Mangalore Electricity Supply Company (MESCOM) Ltd., Ajjampura, India. His research interests include high frequency soft-switching converters for power generation from renewable energy sources and their grid interfacing applications.

Venkatesaperumal B. received the B.E. degree in electrical engineering from Madras University, Chennai, India, in 1999, the M.E. degree in power electronics and drives from Bharathidasan University, Tiruchirappalli, India, in 2001, and the Ph.D. degree in electrical engineering from the Indian Institute of Technology Delhi, New Delhi, India, in 2007.

He was a Technical Leader with GE, Schneider Electric, Power Electronic R&D Division, and SunEdison, Bangalore, India. He is currently a Professor with the Department of Electrical and Electronics Engineering, National Institute of Technology, Surathkal, India. His research interests include applications of power electronics in health care, solar generation, and brushless generation.